15

Walking Pattern Generation and Stabilization of Walking for Small Humanoid Robots

Yogo Takada, Tomoki Tajiri, Kiyoshi Ogawa and Tomoyuki Wakisaka
Osaka City University
Japan

1. Introduction

Declining birthrate and a growing proportion of elderly people are closed up as social issues in Japan. Especially, a growing proportion of elderly people is seen as an issue in nations of Europe and North America and so on as well as Japan. New labors engaging in the life support and the nursing for the elderly person will need in the future. To supplement the lack of the manpower, the research that applies the robot technology to the welfare field is important. Especially, because the shape of a humanoid robot looks like human, the person who receives nursing can be relieved. Besides, a humanoid robot can act under person's life environment, and can use the tool that the person uses. In addition, it is possible to avoid colliding with something put on the ground because the biped robot does not move with wheels. The biped robot can be used even in the environment including steps and ruggedness where robots with wheels cannot be used. In a word, the biped humanoid robot is extremely effective as the robot that acts in the environment where we live in daily life.

However, it is necessary to prevent the robot from falling in the case of two-legged locomotion. Moreover, it is also necessary to keep controlling while the robot is only standing with stable posture. Various techniques about the walking of a humanoid robot have been devised up to now in recent years, and the walking pattern generation of a humanoid robot with complex dynamics has become possible.

On the floor where information about the height of the small step was obtained beforehand, steady dynamic walking was achieved by using such as the technique of linear inverse pendulum model where the humanoid robot was expressed with an inverted pendulum of simple single-mass system, and truck model with preview control of ZMP trajectory (Kajita, 2005, 2009). However, in the case that the robot walks in a real environment, it is difficult to obtain the detailed information on the floor beforehand and give the information to the biped robot at any time. There are research examples (Kajita & Tani., 1996) of making the robot measure the shape of the road with sensors while walking. But, it is necessary to install the highly accurate sensor in the robot. The road where the robot walks is not only a smooth road. A small ruggedness and a gradual inclination are contained in many cases. However, it is impossible to record information of detailed shape on the ruggedness onto the robot beforehand.

A biped robot KHR-2HV manufactured by Kondo Kagaku Co., Ltd. in Japan and HOAP-1 manufactured by Fujitsu Automation Ltd. in Japan were used in this study as humanoid robots. The basic walking experiment was conducted by using KHR-2HV. Then, another

biped robot HOAP-1 was used in the attempt of steady gait on the floor including unknown ruggedness. ZMP (Zero Moment Point) that shows dynamic stability is used in a lot of biped robots, and it is important to plan the position trajectory of the ankles and waist beforehand when walking. The locomotory controller for walking, running, swimming and flying animals is based on a Central Pattern Generator (CPG). Models of CPGs have been proposed and many roboticists have adapted these models for the control of robots (Miyakoshi et al., 2000).

In this study, first, by using KHR-2HV, posture control based on ZMP was attempted and the walking posture was stabilized. A simple nervous oscillator circuit was composed based on CPG and the reflex. We tried to stabilize the walking state with posture control by using ZMP, after the walking pattern was generated with CPG.

Next, by using HOAP-1, we tried the dynamic walking of the biped robot when there is ruggedness on the floor. Dynamic walking is more efficient than static walking. But, the dynamic walking is not steady when ruggedness exists on the floor. Therefore, various devices need to control. The walking pattern composed of each joint angle is also necessary for the dynamic walking of biped robot. Linear inverse pendulum mode is used to make the walking pattern. And, the position-based impedance control was conducted to soften the impact caused by the collision of a rugged floor and foot. In this impedance control, the signals from the force sensors installed on the soles were used. In addition, the upper part of the robot was controlled by using the output signals of the gyro sensor and acceleration sensor to correct the inclination when the posture inclined. We verified whether the robot was able to walk stably on the road on which there was unknown ruggedness by applying these methods to the control of robot by using a physical simulator and an actual robot HOAP-1.

2. Stabilization of static walking by use of CPG

Walking of biped robots greatly is distinguished between static walk and dynamic walk. The static walk is described here. At the present time, ZMP (Zero Moment Point) that shows dynamic stability is used in a lot of robots, and the trajectory plans of walking are studied. Moreover, on the other hand, the robots walk with motion generation techniques of rhythm pattern generator CPG (Central Pattern Generator) and the reflex motion by the sense referring creature models.

In this study, first, only the ZMP was used to control the posture. Then, the stabilization with ZMP and the gait pattern generated with the CPG and reflex motion were combined to achieve steadier walking.

2.1 Small humanoid robot

Robot KHR-2HV manufactured by Kondo Kagaku Co. was used for this study. The height is 0.35 m and weight is 1.26 kg. This robot is shown in Fig. 1.

The number of degrees of freedom in the upper part of the body is 7, and that of legs is 10, and the total is 17. The force sensors (made of Inaba Rubber Co, Ltd.) were arranged in each of four corners of the sole of foot, and the back of humanoid robot was equipped with RM-board made of iXs Research Corp. as a controller.

For the simulation of robot motion, open architecture kinetic simulator OpenHRP (Kanehiro et al., 2004), which was an integrated software development environment for humanoid robotics, was used. The simulation model is based on KHR-2HV with the above-mentioned equipments. The sampling period of simulation in this study was set to 140 ms.

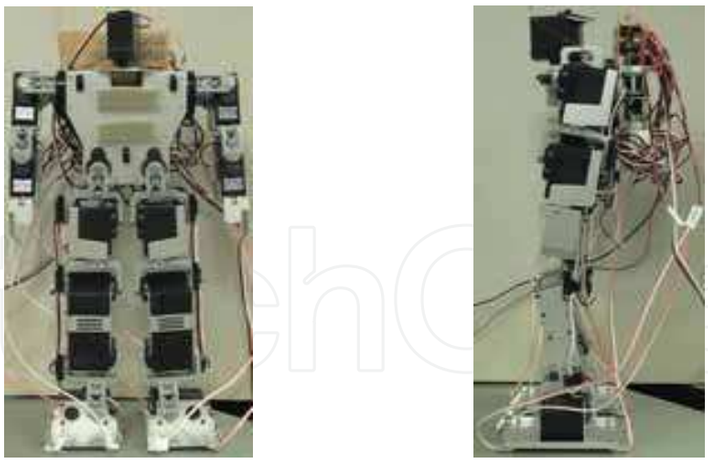

Fig. 1. Photographs of humanoid robot KHR-2HV

2.2 Motion control technique of humanoid robot

The motion control is necessary in order to make the robot KHR-2HV walk. Figure 2 shows the method of the motion control for the robot.

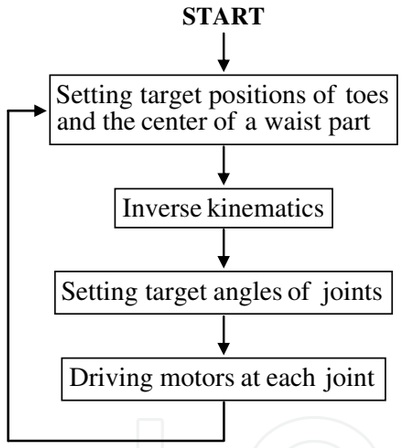

Fig. 2. Motion control technique of humanoid robot

It is important to set target positions of toes and the center of a waist part so as to make the robot move ideally. The target angle of each joint is obtained with the reverse kinematics. Then, each joint is controlled to target joint angle with motor servo control. Consequently, the toes and waist operate ideally, and the stable walking of the robot is achieved. However, in the simulation, the servo control of each motor was not considered. It was assumed that each joint moves in the sampling period to the target angle in this simulation.

2.3 Walking control using ZMP

ZMP is a point on the floor surface where the inertia force and moment produced by gravitation become zero, and it deeply relates to the cause of a tumble while the robot is walking. ZMP is known to be equivalent to a central point of the reaction force from the floor. In this study, ZMP was obtained as the central point calculated from force sensors

installed on the sole of foot. The ZMP calculated from the value of the sensor was used for the posture control of the robot shown in Fig. 3. This control system is two degree of freedom PID controller that makes ZMP obtained from the force sensors approach to the target trajectory of robot. The heaviest waist in robot is controlled based on the value of error between the position of ZMP p_{ZMP} while walking and the target of ZMP $\tilde{p}_{ZMP}$. Because ZMP p_{ZMP} approaches the target ZMP, the robot stabilizes its posture. The renewal amount of the waist position Δp_{waist} is given by Equation 1,

$$\Delta p^n_{\mathrm{waist}} = K_{\mathrm{p}}\left[\left\{(1-\alpha)\tilde{p}^n_{\mathrm{ZMP}} - p^n_{\mathrm{ZMP}}\right\} + \frac{1}{T_{\mathrm{I}}}\sum_{i=0}^{n}\left(\tilde{p}^i_{\mathrm{ZMP}} - p^i_{\mathrm{ZMP}}\right)\Delta T\right.$$

$$\left. + T_{\mathrm{D}}\frac{\left\{(1-\beta)\tilde{p}^n_{\mathrm{ZMP}} - p^n_{\mathrm{ZMP}}\right\} - \left\{(1-\beta)\tilde{p}^{n-1}_{\mathrm{ZMP}} - p^{n-1}_{\mathrm{ZMP}}\right\}}{\Delta T}\right] \tag{1}$$

where, Δp^n_{waist} is renewal amount of waist position at the time $n \cdot \Delta T$, ΔT is sampling period, $\tilde{p}^n_{ZMP}$ is target ZMP at $n \cdot \Delta T$, p^n_{ZMP} is measured value of ZMP at $n \cdot \Delta T$.
This posture controller was mounted on the robot, and the walking simulation was conducted. The targeted value of right and left foot toes is given beforehand as a time function.

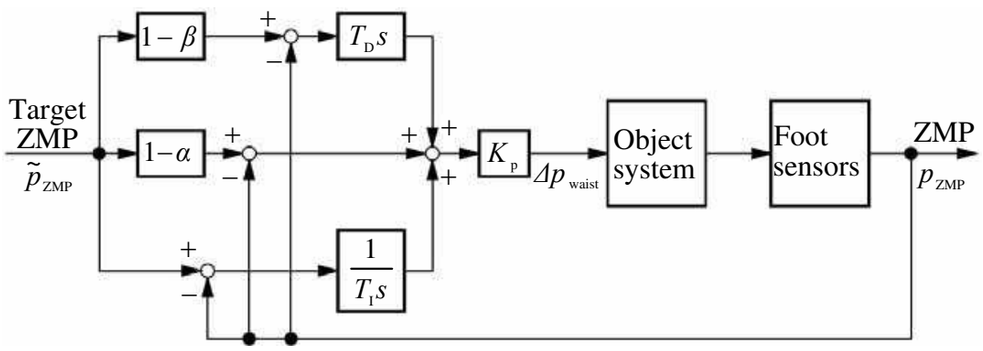

Fig. 3. Posture controller for the robot using ZMP

Figures 4 and 5 show the appearances and trajectories of the walking robot on the simulation. Fig. 4 displays the robot walking for ten seconds from on the left to lower right at intervals of one second. Moreover, the X direction shows travelling direction of robot, and the Y direction shows the lateral direction of robot respectively. The robot did not fall as a result of mounting the posture controller in which the waist center position was controlled to make ZMP approach to the target ZMP trajectory. The robot kept walking stably. The ZMP follows the target in both X direction and Y direction. It is effective in the stabilization of the biped robot walking to operate the heaviest part (waist in this case) in robot.
Though we desperately adjusted the parameters in the posture controller, the parameters that showed a quicker response were not able to be obtained. Therefore, the walking cycle of robot could not shorten any further. Moreover, the waist position of the direction of X has swung to about 15 mm for the period while the idling leg is exchanged with the supporting leg because this control method relies on only the ZMP when the position of the waist is controlled.

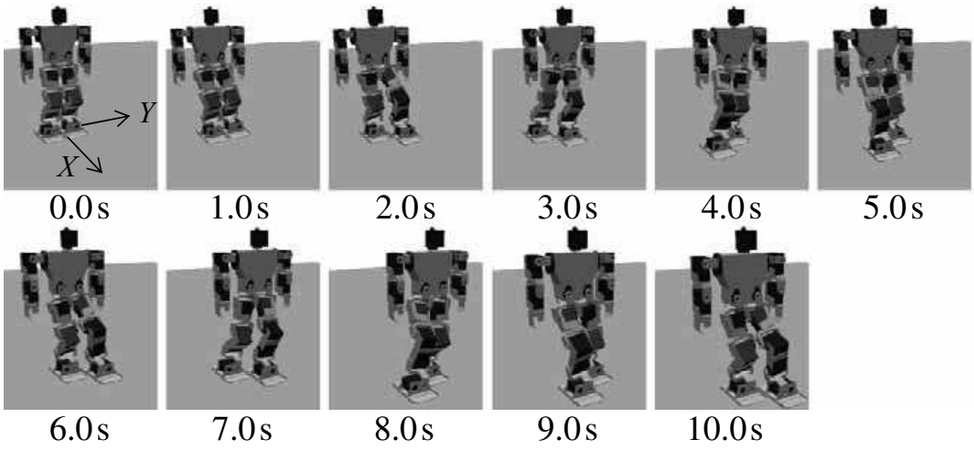

Fig. 4. Appearance of robot walking with posture control by using ZMP

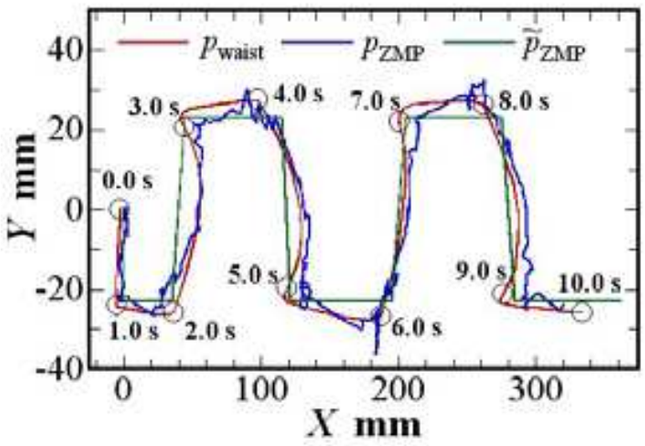

Fig. 5. Trajectories of robot walking with posture control by using ZMP

2.4 Walking pattern generation used CPG and stabilization of walking

2.4.1 Nervous oscillator

In this study, we used a nervous oscillator (Matsuoka, 1985, 1987) composed of adaptable nerve elements (neurons) as the motion generation technique of creature model. The theoretical concept of adaptable nerve elements is given as the following Equations 2 to 5,

$$\tau_{u_i}\dot{u}_i = -u_i - \beta_i v_i + u_i^0 + s_i - \tilde{y}_i \tag{2}$$

$$\tau_{v_i}\dot{v}_i = -v_i + y_i \tag{3}$$

$$y_i = \max(0, u_i) \tag{4}$$

$$\tilde{y}_i = \sum_{j=0,\ldots,N_n-1}^{j\neq i} w_{ij} y_j \tag{5}$$

$$(i = 0,\ldots,N_n - 1) \tag{6}$$

where, N_n is the number of nerve elements, u_i is neuron which shows internal state of nerve element, affixing character i indicates the nerve element of the i th, v_i is variable that shows adaptive effect, y_i is output, s_i is input signal from outside sensor, $\tilde{y}_i$ is variable that shows control from other nerve elements, τ_{ui} is time constant concerning u_i in Equation 2, τ_{vi} is time constant concerning v_i in Equation 3, β_i is variable that shows frequency where adaptation is caused, u_i^0 is steady input, w_{ij} is coupling coefficient from nerve element j th to nerve element i th. When w_{ij} is positive, $\tilde{y}_i$ works as an inhibitory signal. And, when w_{ij} is negative, $\tilde{y}_i$ works as an excitatory signal.

The nervous oscillator has the basic structure where adaptable nerve elements that united to control the other nerve elements mutually. The basic structure is shown in Fig. 6. Because the CPG model with this nervous oscillator changes flexibly the rhythm pattern according to the input signal that come from the outside, the flexible walking can be achieved. Figure 7 shows the behaviour of basic nervous oscillator of Fig. 6. Here, u_i^0 =2.5.

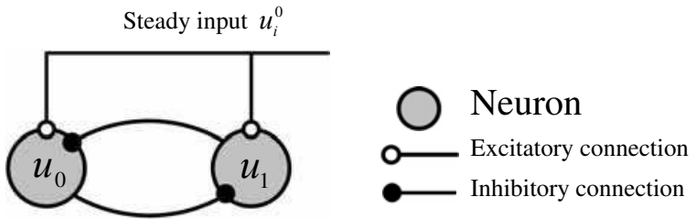

Fig. 6. Structure of nervous oscillator

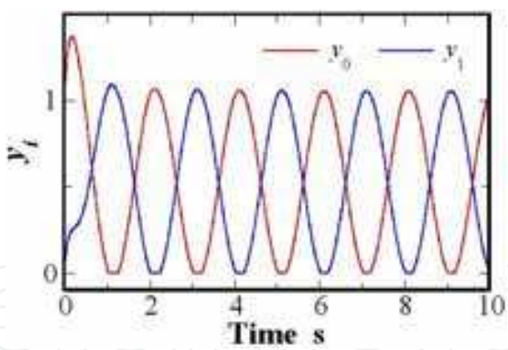

Fig. 7. Output signals from nervous oscillator

Both values y_0 and y_1 rise because of the regular input value at the time of the start. When the nerve element with strong excitement controls the other side by mutually controlling effect, the excitement on the controlled side cools down. However, when the excitement level of the other element is low, the excitement of nerve element becomes stronger. But, the excitement cools down by own adaptive effect. Besides, the other nerve element begins to get excited because the inhibitory power becomes weak when the excitement cools down. Therefore, the phase lag arises between two output signals. Then, a periodic output can be obtained. The gait pattern is generated with the use of such a periodic output to the targeted value of the robot. This is a basic idea of the nervous oscillator with CPG.

2.4.2 Walking pattern generation used CPG

Figures 8 and 9 show the nervous oscillator circuit used for the robot walking. The output signals y_0, y_1 of the nervous oscillator composed of u_0, u_1 in main generator in Fig. 8 were used for the position control of the waist center for the lateral direction. In a word, the walking rhythm of robot was generated with CPG. The outputs y_2, y_3 of the nerve elements u_2, u_3 uniting main generator with excitatory connection were used for the target height of right and left legs' toe. These nerve elements were controlled by the input step signals s_2, s_3. Working of these nerve elements has improved timing of exchanging the supporting leg and the idling leg. Therefore, the robot steps (does walking motion in a same place) stably.

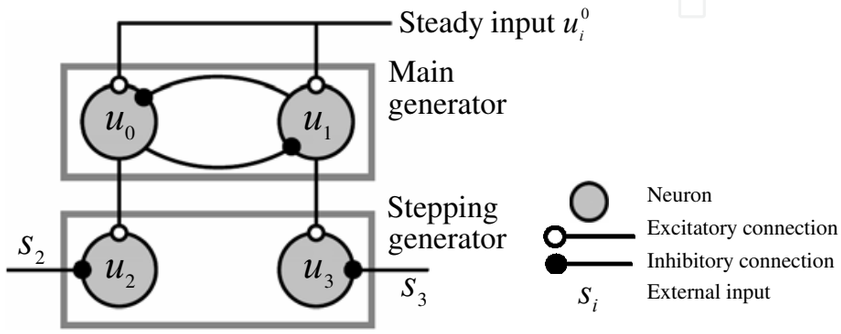

Fig. 8. CPG model for the robot stepping stably

The nervous oscillator composed of u_4, u_5 in Fig. 9, which generates the output signals y_4, y_5 reacting to the input signals s_4, s_5 from force sensors on the sole of the foot, is used for the stepping forward. The robot judges whether the sole of foot touches the ground by using the force sensors. The judged result enters the nervous oscillator as an input signal if the sole of foot touches the ground. The nerve element becomes a state of excitation when the signal enters, and the output signal comes out as reflex action. The robot steps forward by using the signal come from the nervous oscillator according to the contact situation with the ground.

Fig. 9. Reflex model for the robot walking forward

Figures 10 and 11 show the appearances and trajectories of the walking robot with CPG on the simulation. Periodic walking operation was achieved based on the rhythm generated by the CPG model. In addition, the robot was able to walk without falling down by adjusting the timing in which the idling leg was exchanged for the supporting leg by external inputs according to ZMP. Moreover, the motions of ZMP and waist for the travelling direction in this method were calmer than the method in the case that only ZMP signal was used with PID control. Even if the walking cycle shortened, a steady walking could be maintained.

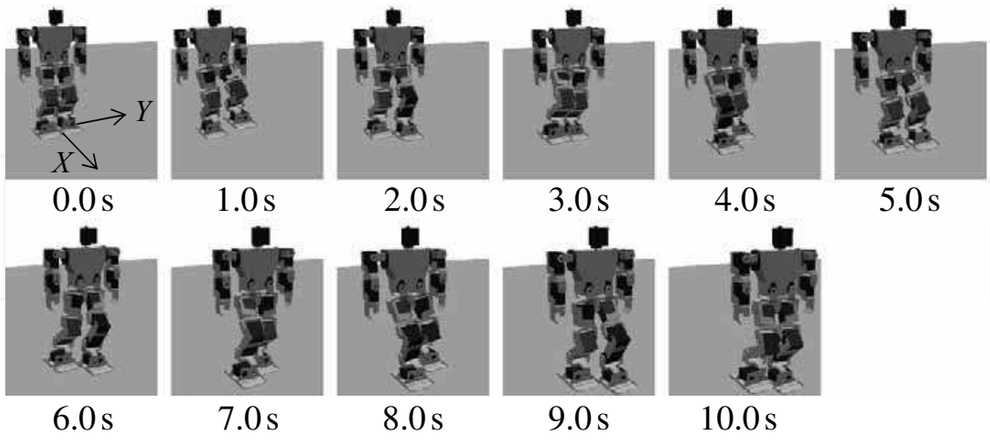

Fig. 10. Appearance of robot walking with CPG and posture control by using ZMP

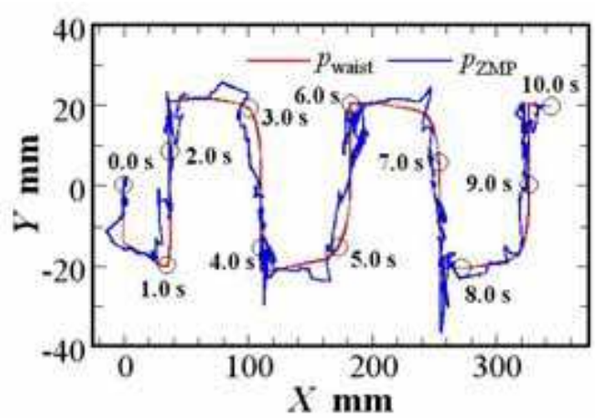

Fig. 11. Trajectories of robot walking with CPG and posture control by using ZMP

2.4.3 Walking experiment by using KHR-2HV

The CPG model used for the walking simulation was applied to a real machine, and the walking experiment was conducted. The gait initiation time of KHR-2HV was after 2.5 s passed from the experiment start. Then, the control period was set to 130 ms. In this time, I/ O waiting time was about 80 ms and the computing time was about 50 ms. Figure 12 shows the appearance of KHR-2HV's walking. Moreover, Figs. 13 and 14 show the time behaviors of the waist position and ZMP. The motion of the travelling direction (X direction) is shown in Fig. 13, and that of lateral direction (Y direction) is shown in Fig. 14. Though the trajectory of ZMP was vibrating, a steady walking could be achieved based on the rhythm generated with the CPG model.

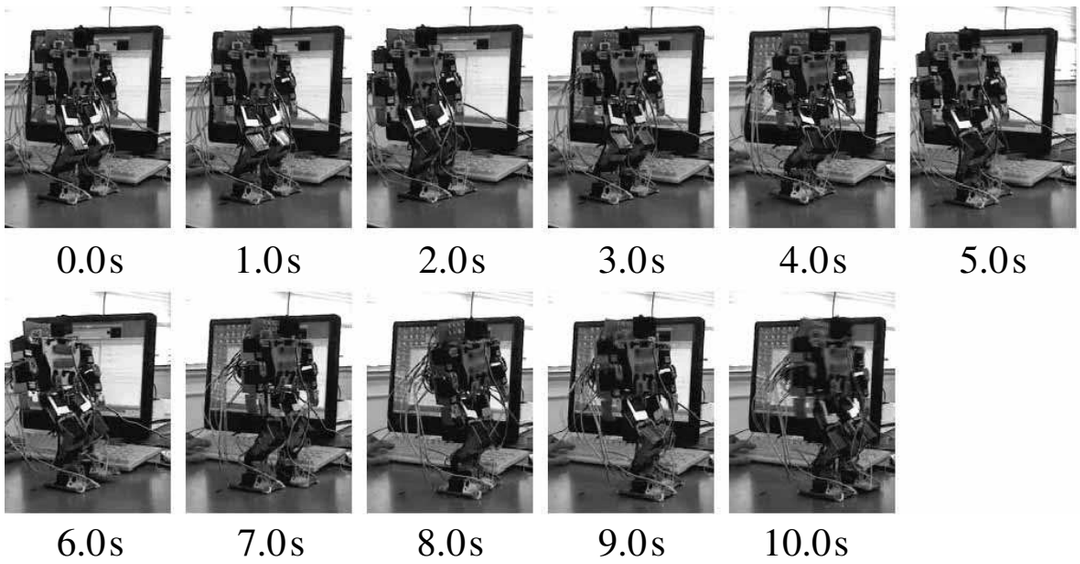

Fig. 12. Appearance of KHR-2HV walking with CPG and posture control by using ZMP

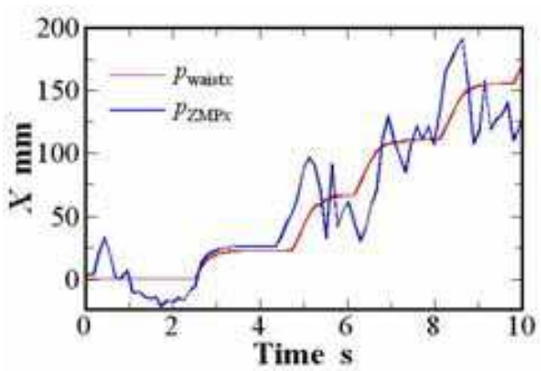

Fig. 13. Trajectories for travelling direction of KHR-2HV walking with CPG and posture control by using ZMP

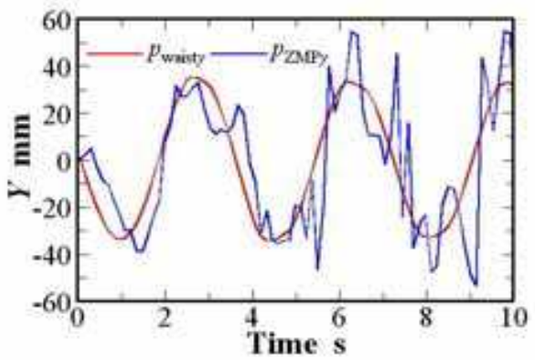

Fig. 14. Trajectories for lateral direction of KHR-2HV walking with CPG and posture control by using ZMP

3. Stabilization of dynamic walking on uneven road

High-speed movement is expected in the dynamic walk compared with the static walk. However, the control system for the dynamic walk is more difficult than that of static walk. We have advanced the research by using more excellent robot HOAP-1 though KHR-2HV had been used till then because the dynamic walk needs a high-integrity controller.

It is necessary to lead the trajectory of the gravity point of a biped robot and predict the landing place of the idling leg beforehand so as to achieve the dynamic walk. It is not difficult to achieve the dynamic walk on the simulation if the theory to predict the landing point is extremely accurate. However, for the success of stable walking in the experiment with a real biped robot, there are conditions that each link of robot is rigid and that floor surface must be completely flat.

In the real environment, minute ruggedness of few millimeters in height exists even if it is a floor surface that looks smooth. The center of gravity of the robot vibrates because of the ruggedness, and the robot falls down. Therefore, it is difficult to achieve the dynamic walk compared with the static walk. Here, the method of achieving a stable dynamic walk is described even if minute ruggedness of several millimeters exists in the floor face.

3.1 Configuration of humanoid robot "HOAP-1"

Biped humanoid robot HOAP-1 was used in this study. Figure 15 shows the photograph of HOAP-1 whose height is 483 mm and weight is 5.9 kg. The number of degrees of freedom in the upper part of the body is 8, and that of legs is 12, and the total is 20. The arrangement of each joint of legs is shown in Fig. 16. Because only 12 motors of the leg were used to walking in this study, the upper part of the body was omitted in this Fig. 16. Two axes in the ankle and three axes in the waist intersect at one point respectively. The parameters of each link are shown in Table 1. The three-axes acceleration sensor and three-axes gyro sensor are installed in the waist. Four force resister sensors are installed in right and left sole of the foot. The resistance of these force resister sensors changes in proportion according to pressure.

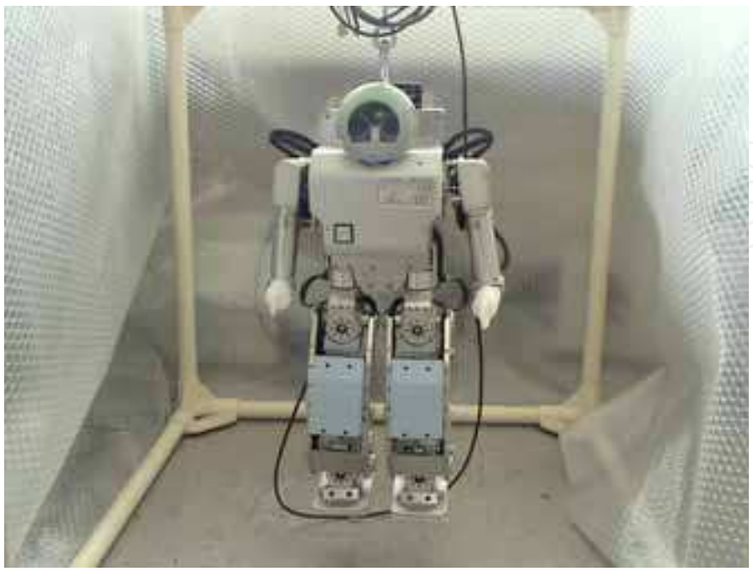

Fig. 15. Photograph of HOAP-1

	Length (m)	Mass (kg)
Leg link 1	L_1 : 0.039	0.04
Leg link 2	L_2 : 0.10	0.46
Leg link 3	L_3 : 0.10	0.46
Leg link 4	L_4 : 0.037	0.14

Table 1. Parameters of each link

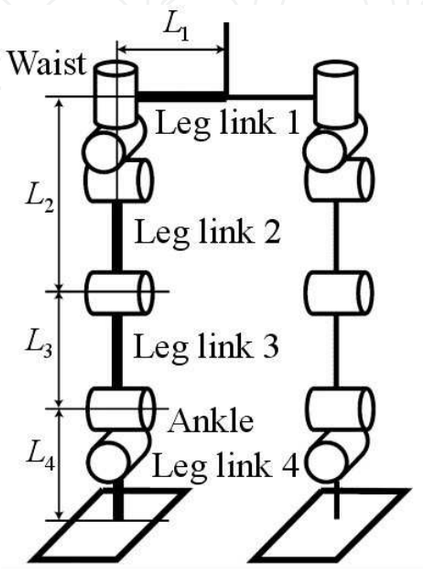

Fig. 16. Arrangement of each joint of legs

3.2 Control system to stabilize the dynamic walk

3.2.1 Position-based impedance control for an idling leg

When the idling leg touches to unknown ruggedness shown in Fig. 17, an actual landing point changes from the one of the planned gait pattern. Then, the impact is generated on the sole of foot when the idling leg touches to the ground. The robot falls down after its posture got worse because this impulsive force becomes very big disturbance in the object system.

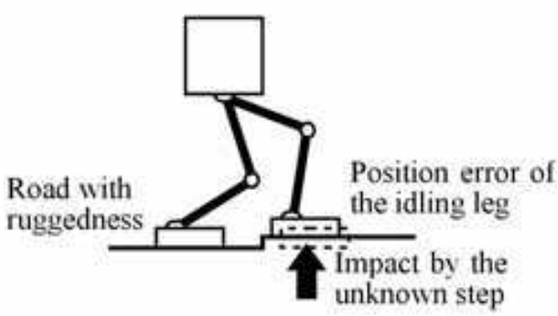

Fig. 17. Walking on a road with unknown step

The impedance control is often used as a technique for controlling the contact strength between the surrounding environment and a part of the robot in the field of the robotic

control. There are some examples in the field of humanoid robot (Kawaji et al., 1996; Sorao et al., 1997; Nisikawa et al., 1999; Hasimoto et al., 2007). In this study, the position-based impedance control was conducted by using the force resister sensors installed on the sole of foot of the robot. In the impedance control, three virtual impedance properties of inertia, rigidity and damping coefficient are given to the part of control object. Then, the amount of the change at the position of ankle is led from the dynamic equation according to the impulsive force measured with the sensors. The impulsive force weakens when the leg moves based on the led position. In a word, it is expected that the impedance control have the same effect as when real springs and dampers are given to the target part.
Four force resister sensors are installed on the each sole of right and left foot of HOAP-1 used in this study, and the arrangement is shown in Fig. 18. In addition, each parameter in Fig. 18 is shown in Table 2.

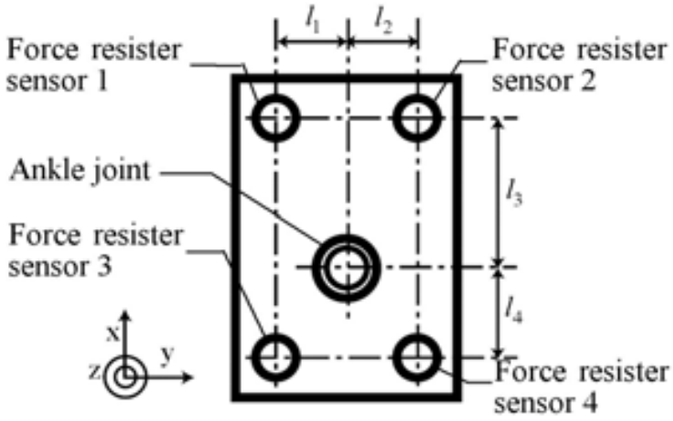

Fig. 18. Arrangement of force resister sensors

	Length (m)
l_1	0.017
l_2	0.017
l_3	0.042
l_4	0.028

Table 2. Parameters for the arrangement of force resister sensors

Only force in the direction of z can be detected with four force resister sensors 1-4, and the forces measured with force resister sensors were defined as f_1, f_2, f_3, f_4 respectively. Torques τ_x, τ_y where the center of gyration is x axis and y axis respectively and force f_z in the direction z can be obtained from Equation 6,

$$\begin{aligned} f_z &= f_1 + f_2 + f_3 + f_4 \\ \tau_x &= (f_1 l_1 + f_2 l_1) - (f_2 l_2 + f_2 l_4) \\ \tau_y &= (f_1 l_3 + f_2 l_3) - (f_3 l_2 + f_4 l_4) \end{aligned} \quad (6)$$

and the virtual spring and damper mechanism shown in Fig. 19 can be utilized for the control system to stabilize the dynamic walk by using the force and torque on the toe of

idling leg obtained by Equation 6. The dynamic equation of this toe of idling leg model is given as Equation 7,

$$\begin{aligned} \boldsymbol{F} &= \boldsymbol{M}_{\mathrm{imp}}\ddot{\boldsymbol{p}}_{\mathrm{leg}} + \boldsymbol{C}_{\mathrm{imp}}\dot{\boldsymbol{p}}_{\mathrm{leg}} + \boldsymbol{K}_{\mathrm{imp}}\boldsymbol{p}_{\mathrm{leg}} \\ \boldsymbol{F} &= \begin{bmatrix} \tau_{\mathrm{x}} & \tau_{\mathrm{y}} & f_{\mathrm{z}} \end{bmatrix}^{\mathrm{T}},\ \boldsymbol{p}_{\mathrm{leg}} = \begin{bmatrix} \theta_{\mathrm{x}} & \theta_{\mathrm{y}} & p_{\mathrm{z}} \end{bmatrix}^{\mathrm{T}} \end{aligned} \tag{7}$$

where, $\mathbf{M}_{\mathrm{imp}}$ (diagonal matrix: $\mathrm{diag}(J_{\mathrm{x}}, J_{\mathrm{y}}, M_{\mathrm{z}})$) is virtual inertia and mass, $\mathbf{C}_{\mathrm{imp}}$ ($\mathrm{diag}(C_{\mathrm{x}}, C_{\mathrm{y}}, C_{\mathrm{z}})$) is virtual viscous coefficient, $\mathbf{K}_{\mathrm{imp}}$ ($\mathrm{diag}(K_{\mathrm{x}}, K_{\mathrm{y}}, K_{\mathrm{z}})$) is virtual coefficient of rigidity, θ_{x} is rotation angle around x axis, θ_{y} is rotation angle around y axis, p_{z} is moving distance in the z direction. In addition, the angle θ_{x}, θ_{y} and moving distance p_{z} are defined to zero on standing upright as shown in Fig. 16, and the arrow direction in Fig. 19 is defined as positive direction.

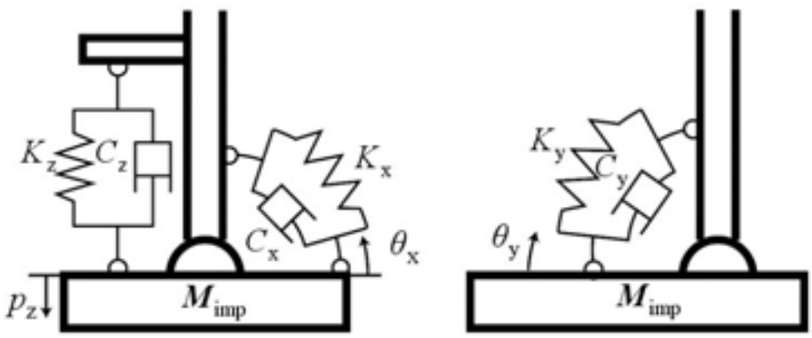

(a) Front view (b) Side view

Fig. 19. Model of impedance control

When the ideal joint angle $\theta_{\mathrm{x}}^{\mathrm{n}}$ around x axis of toe was led by using Equation 7, Equation 8 was obtained,

$$\begin{aligned} A &= K_{\mathrm{x}} + C_{\mathrm{x}} / \Delta t + J_{\mathrm{x}} / \Delta t^2 \\ \theta_{\mathrm{x}}{}^{n} &= \frac{\tau_{\mathrm{x}} + K_{\mathrm{x}}\theta_{x}{}^{0}}{A} + \frac{C_{\mathrm{x}}\theta_{\mathrm{x}}{}^{n-1}}{A\Delta t} + \frac{J_{\mathrm{x}}(2\theta_{\mathrm{x}}{}^{n-1} - \theta_{\mathrm{x}}{}^{n-2})}{A\Delta t^2} \end{aligned} \tag{8}$$

where, θ_{x}^{0} is initial angle (momentary value that the idling leg touch to the ground with unknown ruggedness), $\theta_{\mathrm{x}}^{\mathrm{n}}$ is current angle, $\theta_{\mathrm{x}}^{\mathrm{n-1}}$ is angle before time for 1 period of control period, $\theta_{\mathrm{x}}^{\mathrm{n-2}}$ is angle before time for 2 periods of control period. The rotation angle of toe around y axis and the moving distance in the z direction were controlled as well as x axis.

The impact caused by touching to unknown ruggedness was weakened by impedance control in which the force f_z and torque τ_x, τ_y in Equation 6 were controlled to become small. We verified the effect of impedance control. The parameters in Table 3 were used in this verification. The height of an unknown step on the ground was set to 20 mm. The time behaviors of vertical distance from the waist of the robot to the toe of foot are shown in Fig. 20 as a result. Here, only f_z was applied in the impedance control in this verification. The idling leg's position of the z direction has changed according to the force f_z as shown in Fig. 20. Therefore, it is confirmed that landing point in the z direction of idling leg was corrected in response to unknown step on the ground.

	Value
M_z	1.4 kg
C_z	70.0 Ns/ m
K_z	100.0 N/ m

Table 3. Parameters used in impedance control

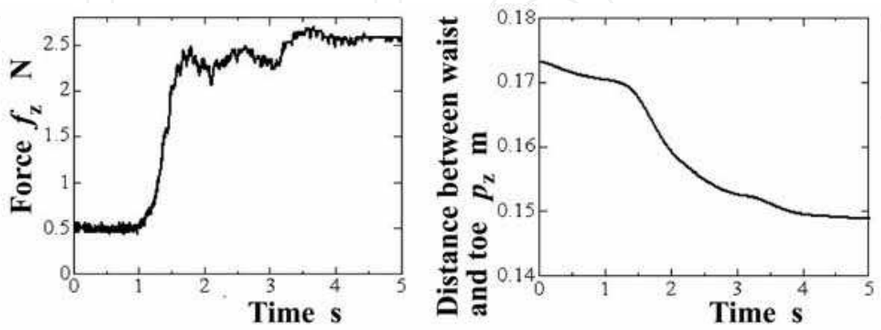

Fig. 20. Time behaviors of force measured with force sensors and distance between waist and toe of foot touching the unknown step on the ground in impedance control

3.2.2 Posture control for upper part of robot

Vertical posture of the upper part in the body is good for steady walking of the biped robot while walking. However, the upper part of the body occasionally inclines as shown in Fig. 21 by the small inclination of floor surface on uneven road. In this case, there is a possibility that ZMP goes out from the stable zone of the foot-ankle assembly. Therefore, when the posture inclined, the upper part of the body must be controlled to keep vertical posture by using the inclination of upper part measured with the gyro sensor and the acceleration sensor. In this posture stabilization control, the motor of the ankle rotated according to the value of the measured inclination.

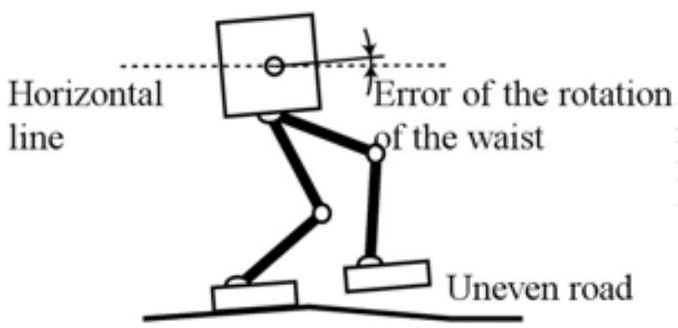

Fig. 21. Walking on a road with slopes

A concrete content is described here. The current inclination of upper part of the body θ_{gyro} was obtained by integrating the output of the gyro sensor installed in the waist of the robot. Then, the upper part of the body was kept vertical by the servo control of the ankle joint according to obtained inclination of the upper part θ_{gyro} and target posture, which was target inclination of upper part $\theta_{\text{target}}^{\text{body}}$.

At this time, target inclination the upper part $\theta_{\text{target}}^{\text{body}}$ was obtained by using the output values a_{x}, a_{y} and a_{z} of the 3-dimensional acceleration sensor installed in the waist of the robot as shown in Equation 9,

$$\theta_{\text{target}}^{\text{body}} = \left[\tan^{-1}(a_{\text{z}} / a_{\text{x}}) \quad \tan^{-1}(a_{\text{z}} / a_{\text{y}}) \right]^{\text{T}} . \tag{9}$$

However, the influence of robot's acceleration is included in the output of this acceleration sensor. Therefore, while the robot has accelerated to the travelling direction, the upper part of the body does not become perpendicular but leans toward the travelling direction a little. This inclination preferably prevents the robot from falling behind, and has stabilized the robot walking more.

The PI controller was used for this posture control as shown in Equation 10,

$$\theta_{\text{ref}}^{\text{leg}} = K_{\text{P}} \left\{ \left(\theta_{\text{gyro}} - \theta_{\text{target}}^{\text{body}} \right) + \frac{1}{T_{\text{I}}} \sum \left(\theta_{\text{gyro}} - \theta_{\text{target}}^{\text{body}} \right) \Delta t \right\} \tag{10}$$

where, K_{P} and T_{I} are parameters of PI controller, and the current inclination of upper part θ_{gyro} is obtained from Equation 11,

$$\theta_{\text{gyro}} = \sum \omega_{\text{gyro}} \Delta t \tag{11}$$

where, ω_{gyro} is angular velocity of the waist obtained from the output of the gyro sensor. The initial posture angle of the robot needed in Equation 11 was obtained after the acceleration sensor outputs when the robot was fixed to flat surface floor were substituted for Equation 9. The posture of robot is controlled so that θ_{gyro} can approach $\theta_{\text{target}}^{\text{body}}$ by the PI controller shown in Equation 10.

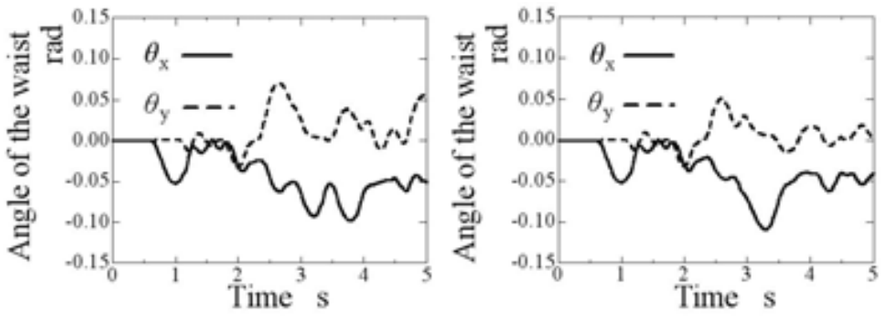

(a) Without PI controller (b) With PI controller

Fig. 22. Inclination angle of the waist

Figure 22 shows the time behaviors about the inclination of the upper part (waist) of the body. The robot walked on the sloping road that is inclining on 2.0°(0.035 rad) in the direction around y axis. The inclination of the upper part was obtained by integrating the output of the gyro sensor. In Fig. 22(a), the time behaviors of robot walking without feedback by the PI control are shown. In Fig. 22(b), the time behaviors in case where inclination angle of upper part was controlled by the PI controller are shown. The robot began walking at 0.5 seconds, and it began to go up on the slope at 2.0 s in both cases.

When there was no posture control, inclination angle in the travelling direction θ_y was 0.02 rad on the average, and the dispersion was 0.024 rad. When there was the posture control, the average was 0.009 rad and the dispersion was 0.017 rad. It was confirmed that the posture of robot was improved as a result of the PI controller.

3.3 Walking on road with ruggedness

3.3.1 Generation of gait pattern with inverse pendulum model

Linear inverse pendulum model (Kajita, 2005) was used for the walking pattern generation in this study. For the linear inverse pendulum model, a robot is assumed to be a single-mass system as shown in Fig. 23, and the dynamic equation of the mass system inverse pendulum model is set up. The trajectory of gravity point in a robot for a steady walking is calculated by solving the dynamic equation about the mass system of inverse pendulum. Adjustment of kick force f prevents the gravity point from falling, and gravity point can be fixed to arbitrary height (Z_c) in Fig. 23. For the linear inverse pendulum model, the trajectory of gravity point while walking can be obtained by setting the walking cycle and the landing position of idling leg beforehand. In this study, relative values as shown in Fig. 24 from a present landing position to the next landing position must be decided. The next landing points are calculated by using Equations 12 and 13 whenever the foot lands on ground,

$$p_x^{(i+1)} = p_x^{(i)} + S_x \tag{12}$$

$$p_y^{(i+1)} = p_y^{(i)} + (-1)^i S_y \tag{13}$$

where, $p_x^{(i)}$ and $p_y^{(i)}$ show x coordinate and y coordinate at the landing point of i th step.

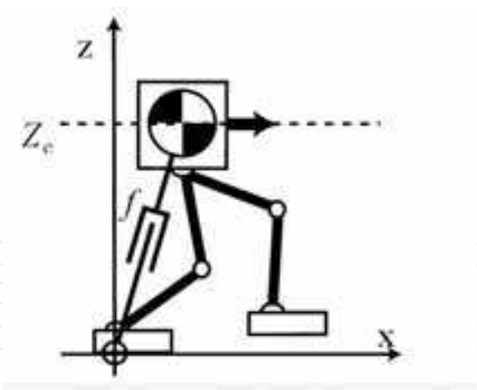

Fig. 23. Liner inverse pendulum model (LIPM) for humanoid robot walking

It is possible to divide into two time period (one-legged support period and two-legged support period) in the walking cycle of human. However, the linear inverse pendulum model is a trajectory plan method only for the one-legged supporting period. Therefore, it is necessary to consider another trajectory plan of gravity point for two-legged supporting period. In this study, in order to connect two-legged supporting period to other one-legged supporting period smoothly and continuously, the positions, velocities and accelerations of gravity point were interpolated by the fifth function.

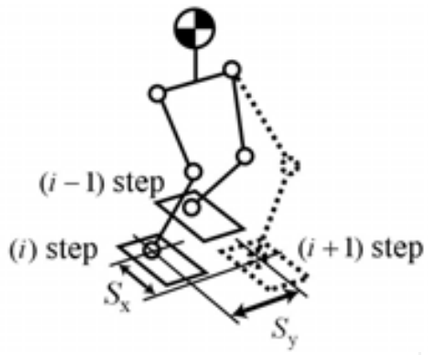

Fig. 24. Parameters used in LIPM

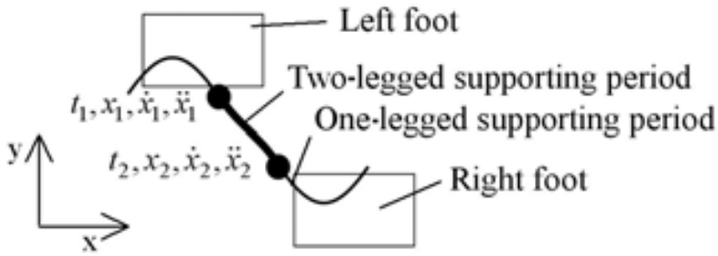

Fig. 25. Connection of two-legged supporting period and one-legged supporting period concerning trajectory of gravity point

The positions, velocities, accelerations and times of gravity point at the start and end of two-legged supporting period were decided beforehand. The trajectory of gravity point $x(t)$ for the two-legged supporting period was obtained by interpolating them with the polynomial equation shown in Equation 14,

$$x(t) = a_0 t^5 + a_1 t^4 + a_2 t^3 + a_3 t^2 + a_4 t + a_5 \tag{14}$$

where, the coefficients from a_1 to a_5 are obtained by Equation 15,

$$\begin{bmatrix} a_0 \\ a_1 \\ a_2 \\ a_3 \\ a_4 \\ a_5 \end{bmatrix} = \begin{bmatrix} {t_0}^5 & {t_0}^4 & {t_0}^3 & {t_0}^2 & t_0 & 1 \\ t_1^5 & t_1^4 & t_1^3 & t_1^2 & t_1 & 1 \\ 5t_0^4 & 4t_0^3 & 3t_0^2 & 2t_0 & 1 & 0 \\ 5t_1^4 & 4t_1^3 & 3t_1^2 & 2t_1 & 1 & 0 \\ 20t_0^3 & 12t_0^2 & 6t_0 & 2 & 0 & 0 \\ 20t_1^3 & 12t_1^2 & 6t_1 & 2 & 0 & 0 \end{bmatrix}^{-1} \begin{bmatrix} x_1 \\ x_2 \\ \dot{x}_1 \\ \dot{x}_2 \\ \ddot{x}_1 \\ \ddot{x}_2 \end{bmatrix}. \tag{15}$$

Moreover, the gravity point trajectory of y-axis $y(t)$ was similarly interpolated and obtained. The trajectories of right and left idling legs were created based on Equation 16,

$$x(t) = x_1 + \frac{S_x}{2}\left(1 - \cos\frac{\pi t}{T_{one}}\right)$$
$$z(t) = \frac{h}{2}\left(1 - \cos\frac{2\pi t}{T_{one}}\right) \quad (16)$$

where, it is necessary to decide the maximum value of height h, the stride S_x and the time for one-legged supporting period T_{one} to obtain $x(t)$ and $z(t)$. Each trajectory was calculated every time, when a present leg left the ground, and it moved to the following planned landing position. By using the Equation 16, the movement of foot, where the acceleration of the idling leg is gradual at beginning and at landing, can be realized as shown in Fig. 26.

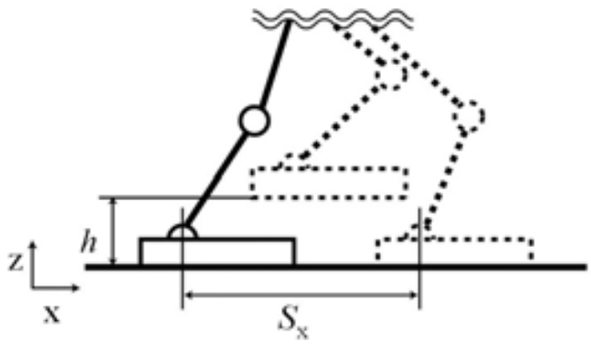

Fig. 26. Movement of idling foot

3.3.2 Walking on ruggedness road in simulation

In the dynamic walk, stable walking can be achieved by applying the gait pattern based on the theory to predict the landing point by using liner inverse pendulum model. However, there are conditions that each link of robot is rigid and that floor surface must be completely flat. In addition, it is necessary to use high-precision actuator systems that operate by target signals. In the real environment, minute ruggedness of few millimeters in height exists even if it is a floor surface that looks smooth. When robots walk on the ruggedness, the gravity point of the robot vibrates because of the ruggedness, and the robot falls down. Therefore, the gait pattern has been improved by using the stabilization control system that describes ahead. Figure 27 shows the outline of the walking control system. Trajectory $\boldsymbol{p}^{COG}$ of the gravity point of robot and trajectory $\boldsymbol{p}_{ref}^{leg}$ of the idling leg were generated with the walking pattern generator. The trajectory of the idling leg was calculated by the impedance control system and becomes $\boldsymbol{p}_{target}^{leg}$. Then, θ_{ref} is calculated with the inverse kinematics. After θ_{ref}^{leg} calculated by the PI controller is added to θ_{ref}, angle θ_{target} becomes target angle vector of all of motors of joints.

The trial of robot walking on the road including unknown ruggedness was conducted with using these walking-pattern generation and stabilization control system on the simulation. OpenHRP (Kanehiro et al., 2004), which was an integrated software development environment for humanoid robotics, was used for the simulator. The time interval of simulator was set to 1 msec, and the control cycle of robot was set to 5 msec. Then other parameters in this simulator are shown in Table 4. Figure 28 shows the size concerning an

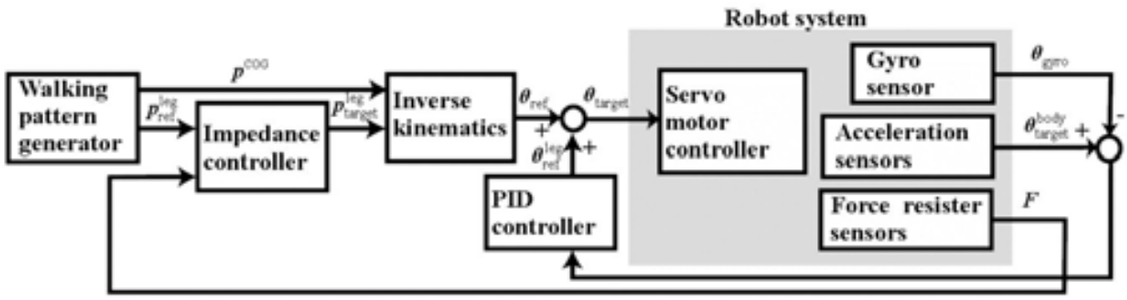

Fig. 27. Outline of walking control system for HOAP-1

LIPM	
	Value
T_{one}	0.3 s
T_{two}	0.2 s
S_x	0.06 m
S_y	0.04 m
h	0.02 m
Z_c	0.13 m

Impedance controller	
	Value
J_x , J_y	1.0 kgm^2
M_z	1.0 kg
K_x , K_y	100.0 Nm/ rad
K_z	1.0 N/ m
C_x , C_y	70.0 Nms/ rad
C_z	10.0 Ns/ m
K_P	2.5 s^{-1}
T_I	0.8 s

Table 4. Parameters used in liner inverse pendulum model (LIPM) and impedance controller

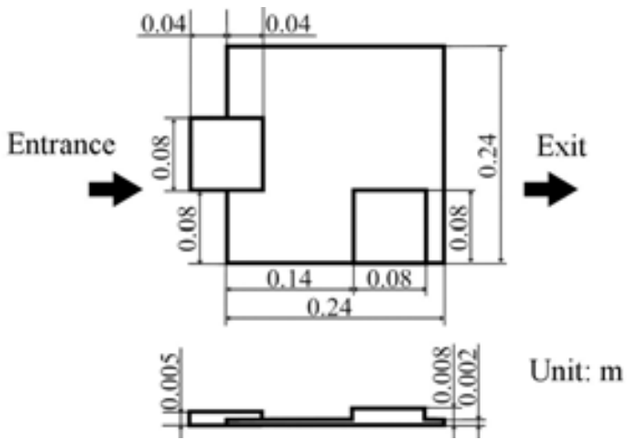

Fig. 28. Unknown ruggedness road used in simulation

unknown ruggedness of the road used in the simulation. The result of walking simulation about the trajectory of the gravity point is shown in Fig. 29 and the trajectory of toe of idling leg is shown in Fig. 30. In this figure, the position of toe of idling leg is appropriately controlled according to the height of unknown step while walking. Figure 31 shows the walking appearance on the simulation with the snap shot of each 0.3 sec. The left leg of the

robot stepped on the ruggedness of 5 mm in height as shown in Fig. 31(e). The robot kept walking on the ruggedness afterwards.

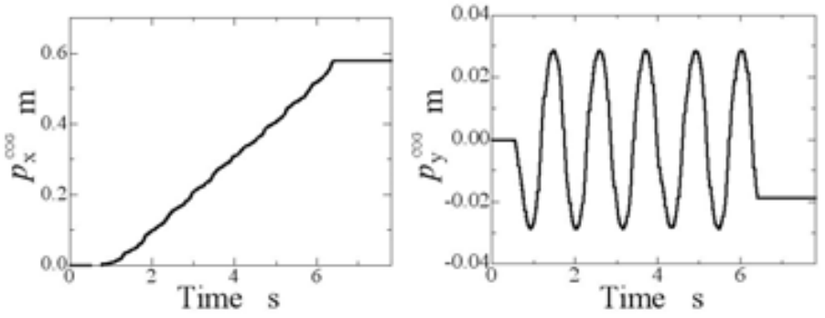

Fig. 29. Time behaviors of COG (center of gravity)

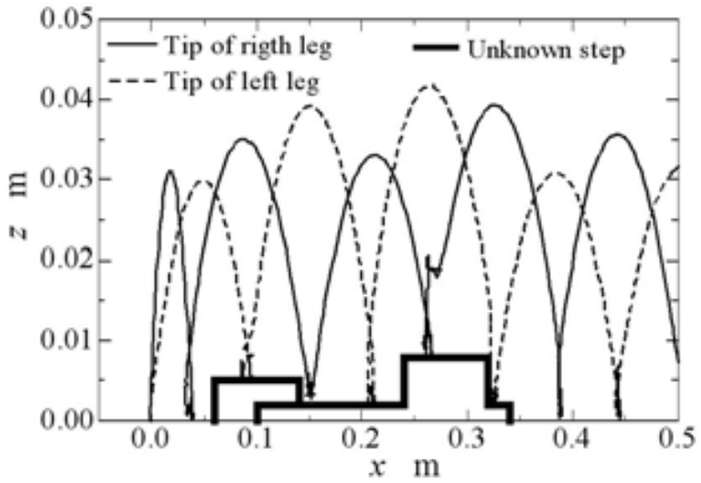

Fig. 30. Trajectory of legs

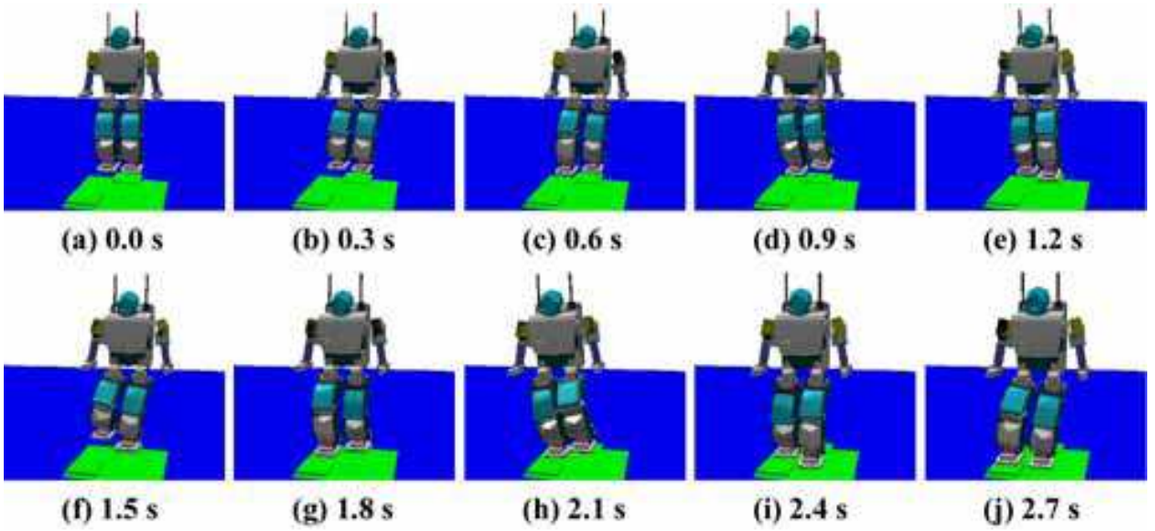

Fig. 31. Snapshots of the walking motion of HOAP-1 on the simulaiton

However, it can be confirmed that the behavior of the right leg did unexpected motion when x reached 0.25 m in Fig. 30. The unexpected motion was generated because the stabilization control system was not able to weaken the impact from an unknown step of 6 mm in height. This walking control is very effective in a real environment because most ruggedness of floor on a smooth road is almost less than 6 mm. Moreover, ruggedness that is higher than 6 mm can be recognized beforehand as an obstacle.

3.4 Experimental verification

This section shows the experimental results of which the previously described control techniques were applied for an actual humanoid robot.

The control cycle was set to 5 msec same as on the simulation, and other control parameters are shown in Table 5. The value of the control parameter is larger than that of the parameters used on the simulation. This is because it was necessary to reduce the value of the parameters in the simulation environment where impact is greater than that of real environment. Because the elastic deformation by the outside force is not considered in the simulation, the calculated impact becomes greater. The value of parameters in the inverse pendulum model was same as the parameters used in the simulation.

	Value
J_x , J_y	1.0 kgm^2
M_z	1.0 kg
K_x , K_y	5.0 Nm/ rad
K_z	200.0 N/ m
C_x , C_y	10.0 Nms/ rad
C_z	140.0 Ns/ m
K_P	3.0 s^{-1}
T_I	1.1 s

Table 5. Parameters used in controller

Moreover, the acrylic boards of 4 mm and 6 mm in thickness were arranged as unknown ruggedness like Fig. 32. The experimental result concerning the trajectory of the gravity point is shown in Fig. 33. The time behavior of the length between the toe of idling leg and waist is shown in Fig. 34. The distance from the toe of idling leg to the waist changes in the range from 0.14 to 0.18 m. The vertical movement of idling foot of the robot is remarkably seen in this Figure. Moreover, points from a to d in this Figure indicate the moment of landing of idling foot. In a word, it can be confirmed that the value of P_z changes a little by landing of the idling foot.

The walking appearance of the real robot HOAP-1 is shown in Fig. 35 as snap shot of photographs. In Fig. 35(a), the right leg is on the acrylic board of 6mm, and the left leg is on another acrylic board of 4mm. Then, in Fig. 35(d), the right leg stepped acrylic board of 4mm on which the left leg was stepping. Afterwards, the robot kept walking stably.

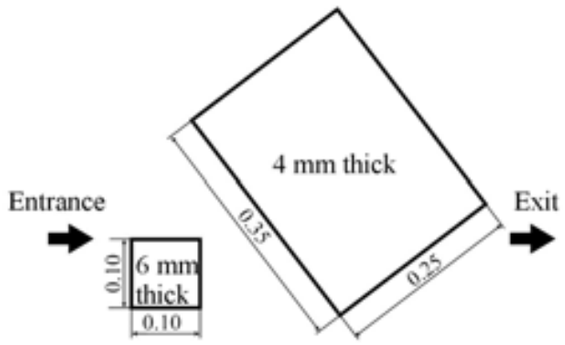

Fig. 32. Arranged acrylic boards of 4 mm and 6 mm as unknown ruggedness

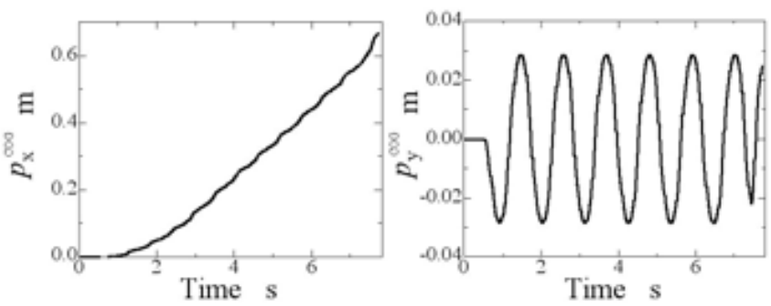

Fig. 33. Trajectory of gravity point of HOAP-1 obtained by experiment

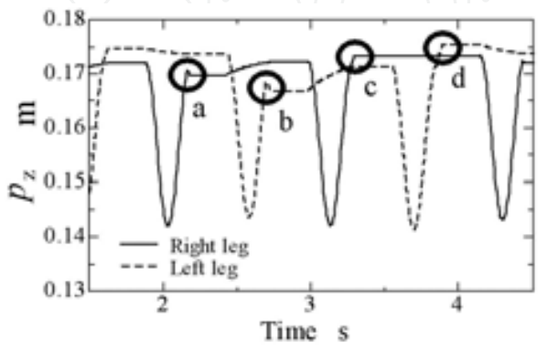

Fig. 34. Trajectory of legs obtained by experiment

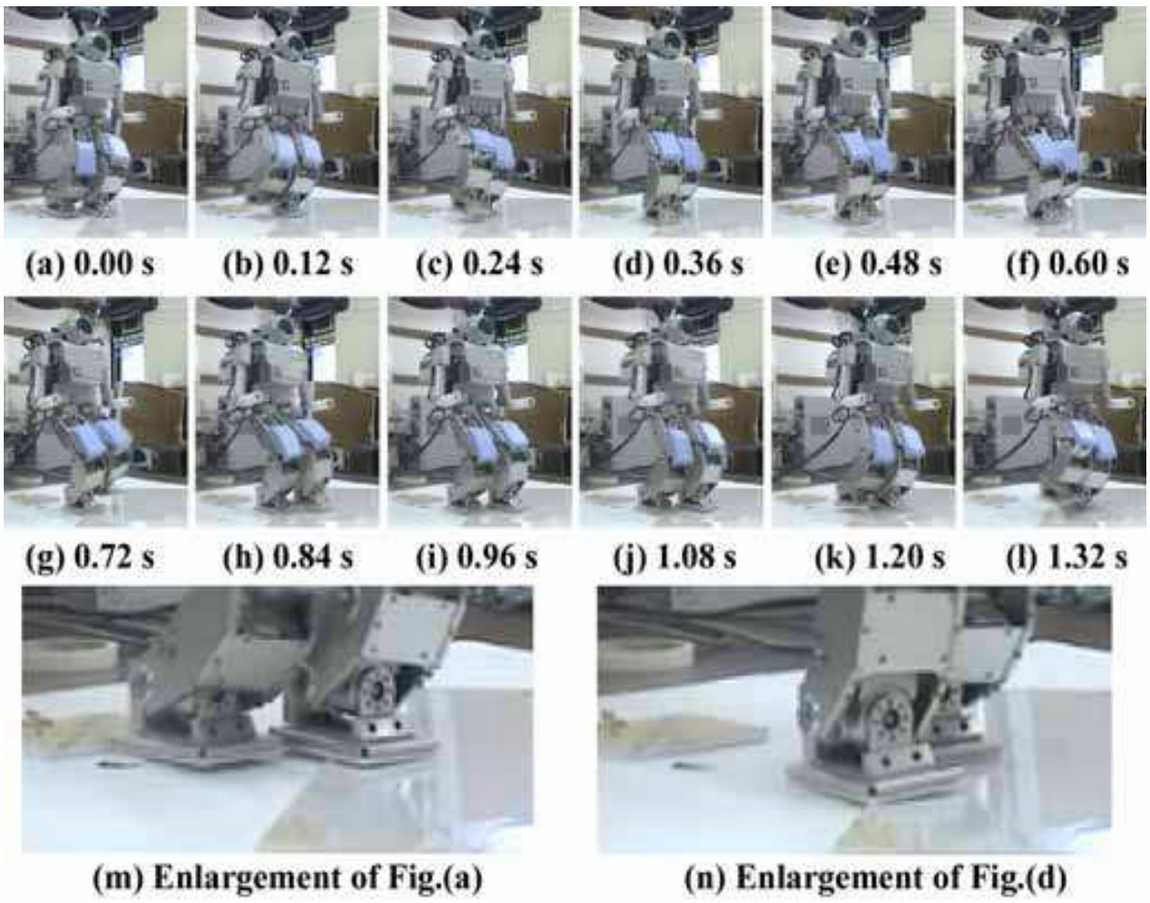

Fig. 35. Arranged acrylic boards of 4 mm and 6 mm as unknown ruggedness

4. Concluding remarks

By using KHR-2HV, posture control based on ZMP was attempted and the walking posture was stabilized. As a result, the robot voluntarily adjusted the exchange timing of supporting leg and idling leg according to the state of robot by using the nerve oscillator circuit. Then, the robot walked controlling posture by using ZMP without the tumble in the simulation. In addition, the CPG model used for the walking simulation was applied to a real biped robot, and the walking pattern was generated. The biped robot KHR-2HV kept walking and maintaining steady balance for a few seconds. But, in this case, KHR-2HV walked slowly with static walking.

Then, by using HOAP-1, we tried the dynamic walking of the biped robot when there is ruggedness on the floor. The biped robot maintained the stability even if the foot collided to the small step from which information was not given, by correcting the position and turning angle of tip of idling leg with the impedance control. In addition, walking steady has been possible as a result of the experiment with a real biped robot HOAP-1 by these control techniques.

5. References

Hasimoto, K., Sugahara, Y., Kawase, M., Hayashi, A., Tanaka, C., Ohta, A., Sawato, T., Endo, N., Lim, H. & Takanishi, A. (2007). *Journal of the Robotics Society of Japan*, Vol.25, No.6, pp. 53-60

Kajita, S., (2005). *Humanoid Robot*, Ohmsha,ISBN4-274-20058-2, Japan

Kajita, S. (2009). From Inverted Pendulums to Biped Locomotion -ZMP and Control Theory-, *Journal of the Robotics Society of Japan*, Vol.27, No.4, pp. 392-395

Kajita, S. & Tani, K. (1996). Control of Dynamic Biped Locomotion Based on Realtime Sensing of the Groung Profile, *Journal of the Robotics Society of Japan*, Vol.14, No.7, pp.1062-1069

Kanehiro, F., Hirukawa, H. & Kajita, S. (2004). OpenHRP: Open Architecture Humanoid Robotics Platform, *The International Journal of Robotics Research*, Vol.23, No.2, pp. 155-165

Kawaji, S., Ogasawara,K. & Iimori, J. (1996). Biped Locomotion Control with Compliance, *IEEJ Transaction on Industrial Applications*, Vol.116-D, No.1, pp. 11-18

Matsuoka, K. (1985). Sustained Oscillations Generated by Mutually Inhibiting Neurons with Adaptation, *Biological Cybernetics*, Vol.52, pp. 367-376

Matsuoka, K. (1987). Mechanisms of Frequency and Pattern Control in the Neural Rhythm Generations, *Biological Cybernetics*, Vol.56, pp. 345-353

Miyakoshi, S., Taga, G., Kuniyoshi, Y., & Nagakubo, A. (2000). Three Dimensional Bipedal Stepping Motion using Neural Oscillators, *Journal of the Robotics Society of Japan*, Vol.18, No.1, pp. 87-93

Nisikawa, N., Fujimoto, Y., Murakami, T. & Ohnishi, K. (1999). Variable Compliance Control for 3 Dimensional Biped Robot considering Environmental Fluctuations, *IEEJ Transaction on Industrial Applications*, Vol.119-D, No.12, pp. 1507-1514

Sorao, S., Murakami, T. & Ohnishi, K. (1997). Walking Control of a Biped Robot by Impedance Control, *IEEJ Transaction on Industrial Applications*, Vol.117-D, No.10, pp. 1227-1233

Biped Robots

Edited by Prof. Armando Carlos Pina Filho

ISBN 978-953-307-216-6
Hard cover, 322 pages
Publisher InTech
Published online 04, February, 2011
Published in print edition February, 2011

Biped robots represent a very interesting research subject, with several particularities and scope topics, such as: mechanical design, gait simulation, patterns generation, kinematics, dynamics, equilibrium, stability, kinds of control, adaptability, biomechanics, cybernetics, and rehabilitation technologies. We have diverse problems related to these topics, making the study of biped robots a very complex subject, and many times the results of researches are not totally satisfactory. However, with scientific and technological advances, based on theoretical and experimental works, many researchers have collaborated in the evolution of the biped robots design, looking for to develop autonomous systems, as well as to help in rehabilitation technologies of human beings. Thus, this book intends to present some works related to the study of biped robots, developed by researchers worldwide.

INTECH
open science | open minds

InTech Europe
University Campus STeP Ri
Slavka Krautzeka 83/A
51000 Rijeka, Croatia
Phone: +385 (51) 770 447
Fax: +385 (51) 686 166
www.intechopen.com

InTech China
Unit 405, Office Block, Hotel Equatorial Shanghai
No.65, Yan An Road (West), Shanghai, 200040, China
中国上海市延安西路65号上海国际贵都大饭店办公楼405单元
Phone: +86-21-62489820
Fax: +86-21-62489821

IntechOpen